Article

The Impact of Urbanization-Induced Land Use Change on Land Surface Temperature

Afera Halefom [1], Yan He [1], Tatsuya Nemoto [2], Lei Feng [1], Runkui Li [1], Venkatesh Raghavan [2], Guifei Jing [3], Xianfeng Song [1,*] and Zheng Duan [4]

[1] College of Resources and Environment, University of Chinese Academy of Sciences, Beijing 100049, China; aferahalefom12@mails.ucas.ac.cn (A.H.); heyan211@mails.ucas.ac.cn (Y.H.)

[2] School of Science Department of Geosciences, Osaka Metropolitan University, Osaka 558-8585, Japan

[3] School of Space and Earth Sciences, Beihang University, 37 Xueyuan Road, Haidian District, Beijing 100191, China

[4] Department of Physical Geography and Ecosystem Science, Lund University, 223 62 Lund, Sweden; zheng.duan@nateko.lu.se

[*] Correspondence: xfsong@ucas.ac.cn

Abstract: Rapid urbanization can change local climate by increasing land surface temperature (LST), particularly in metropolitan regions. This study uses two decades of remote sensing data to investigate how urbanization-induced changes in land use/land cover (LULC) affect LST in the Beijing Region, China. By focusing on the key issue of LST and its contributing variables through buffer zones, we determined how variables influence LST across buffer zones—core, transit, and suburban areas. This approach is crucial for identifying and prioritizing key variables in each zone, enabling targeted, zone-specific measures that can more effectively mitigate LST rise. The main driving variables for the Beijing Region were determined, and the spatial-temporal relationship between LST and driving variables was investigated using a geographically weighted regression (GWR) model. The results demonstrate that the Beijing Region's LST climbed from 2002 to 2022, with increases of 0.904, 0.768, and 0.248 °C in core, transit, and suburban areas, respectively. The study found that human-induced variables contributed significantly to the increase in LST across core and transit areas. Meanwhile, natural variables in suburban areas predominated and contributed to stabilizing local climates and cooling. Over two decades and in all buffer zones, GWR models slightly outperformed ordinary least squares (OLS) models, suggesting that the LST is highly influenced by its local geographical location, incorporating natural and human-induced variables. The results of this study have substantial implications for designing methods to mitigate LST across the three buffer zones in the Beijing Region.

Keywords: urbanization; land surface temperature; buffer zones; human-induced

1. Introduction

The combined impacts of global warming and urbanization considerably worsen the rises in LST. Both of these interrelated processes have a considerable impact on the natural world, particularly in metropolitan regions [1]. Increasing global warming and growing urbanization are raising LST and changing local climates, potentially exacerbating the effects and rendering metropolitan regions obsolete [2]. Gao et al. [3] utilized urban functional zones to investigate the connection between urban morphology, landscape composition, and LST. They employed local climate zones (LCZ) to reorganize metropolitan areas and offered planning solutions to reduce local warming. The global population is quickly growing. More than 50% of the global population resides in urban areas [4]. Urbanization has a substantial impact on microclimatic oscillations in major European cities, including Berlin, Poznań, Paris, and London, resulting in higher LST [5–8]. This rise in LST caused by urbanization has been connected with alterations to metropolitan

morphology [9]. Metropolitan morphological features, especially land surface cover disparities, have been connected with surface temperature, implying that they have a higher influence on changing the climate [10]. Increased coverage by impermeable surfaces, such as buildings and roads, leads to higher LST in urban areas by reducing evapotranspiration and heat retention. According to the study, every 10% increase in impermeable surface density can result in an LST rise to 0.14 °C [8].

Rapid urbanization in Asia and Africa provides substantial social, economic, and environmental issues [11,12]. It causes major changes in land use and cover, influencing the regional and local environment, specifically land surface temperature, with research showing a clear correlation between expanding urban areas and increasing LST [13–15]. Numerous studies have used remote sensing techniques to investigate the impact of land use and land cover changes on LST. Fu and Weng [16] investigated the effects of LULC changes on LST in Pune City, India. Similarly, Imran and Mehmood [17] studied and investigated the major factors of the metropolitan climate in Lahore, Pakistan, to model and predict LST caused by changes in LULC. Remote sensing techniques have been used to determine changes in LULC and seasonal LST fluctuations in quickly expanding cities such as Bangladesh using artificial intelligence algorithms [18]. Abou [19] assessed the effects of LULC variations on LST over the Toshka Depression, Egypt, resulting from human-caused lake drying. Furthermore, Halder et al. [20] utilized remote sensing and geospatial methodologies to monitor urban growth's impact on urban heat islands in Kolkata, India, and assess the impact of climate change on UHI using LST data. Gupta et al. [21] used spatial metrics and satellite data to show how urbanization affects LST in Shimla and Dehradun, two cities in India's Western Himalayas. Furthermore, Sresto et al. [22] used GIS and remote sensing techniques to determine the LULC indicators and surface temperature variations in Bangladesh's Dhaka district. Guo et al. [23] analyzed MODIS LST data from dry periods in Lagos, Nigeria, to see how global climate change and localized urbanization influence long-term urban LST changes. Kalyan and Pathak [24] conducted research in Gandhinagar, Gujarat, assessing the impact of changes in LULC on LST utilizing Landsat imagery. The change in LULC has also been connected with a significant increase in average LST, owing to population growth and urban development [25–27]. Seun et al. [28] investigated the possible influence of rising urbanization on LST in South-West Nigeria, and Moazzam et al. [29] carried out a case study on Jeju Island, Republic of Korea, to assess the implications of urbanization upon Surface Urban Heat Islands and LST. Srikanth and Swain [30] studied the effects of urbanization on LST changes in a semi-arid megacity (Hyderabad) in India. Du et al. [31] investigated the patterns and drivers of LST and urbanization in Zhengzhou, China, and recommended that PLAND be prioritized in urban development. Chao et al. [32] discovered that urbanization considerably increased LST in Hong Kong, Macao, and Guangdong, but the rise in regional greenness mitigated urbanization-induced warming impacts on air surface temperature. Wang et al. [33] investigated the effects of urbanization on LST and air temperature in China, finding that urbanization contributed more to LST than air temperatures, particularly during the daytime. The urban development of China has brought about a mean LST rise of 0.68 °C, with greater increase rates seen in rapidly growing urban regions such as the Yellow and Yangtze River basins [34]. Chengdu's urbanization has considerably increased mean LST by about 10 degrees Celsius throughout the summer [35]. Urban growth, which increases impervious land surface area, has resulted in a substantial rise in LST, exacerbating the effects of global warming in metropolitan regions [36–38].

Numerous studies emphasize the significance of ecologically conscious urban development, which strikes a balance between sustainability and growth concerns to reduce adverse climate effects [39,40]. These studies consistently show that urbanization amplifies LST through LULC change and provides measures to reduce its impacts. Beijing's spatial heterogeneity has a considerable impact on the LST distribution, as population density, land use patterns, vegetation cover, and urbanization levels vary across places. While some places promote urban growth, others emphasize tree planting and greening activities, resulting in varied patterns in LST. To account for this spatial variability, we used buffer zones to investigate the spatial distribution and heterogeneity of LST in the metropolis. This technique contrasts with earlier research, which largely examined city-wide trends in LST increases. In contrast, our research tries to delve into the spatial details, offering a more concentrated view of the city's LST dynamics. Furthermore, looking at Beijing's approach to regulating LST through urban planning will help us to better comprehend sustainable urban development and guide megacities' LST mitigation methods.

The goal of this study is to assess whether urban expansion in core (downtown) areas, particularly in large cities like Beijing, is balanced by compensating measures such as reforestation in suburban areas, aiming to mitigate LST changes at the local level in response to global warming. Our findings indicate that compensating measures have been undertaken within the research area. However, since global warming is a worldwide challenge, a unified response from all cities and countries is essential. Effective climate change mitigation requires collaborative and coordinated efforts to develop solutions that protect the environment and promote sustainable futures.

Our study employs both global modeling (OLS) and local modeling (GWR) to explore whether the relationship between the dependent variable (LST) and independent variables (natural and human variables) varies across geographic space, indicating spatial homogeneity or heterogeneity. By focusing on the key issue of LST and its contributing variables through buffer zones, we determined how variables influence LST across buffer zones—core, transit, and suburban areas. This approach is crucial for identifying and prioritizing key variables in each zone, enabling targeted, zone-specific measures that can more effectively mitigate LST rise.

1.1. Beijing's Metropolitan

Beijing is located in Northern China, at 39.43–41.05°N and 115.42–117.50°E (Figure 1). It experiences a warm monsoon climate and four distinct seasons, including cold and windy winters and hot and humid summers. Over the last 40 years, the average annual temperature has been 11 °C [36]. A vast semicircular mountainous cove encircles the so-called Beijing Plain, which has an average elevation of approximately 40 m and receives an average yearly precipitation of 600–700 mm [41].

Beijing, with a city history of over 3000 years and a capital history of over 800 years, is modern China's capital and the country's cultural and political hub. Beijing, China's political, cultural, and international communication center, has grown modestly since 1949. This expansion increased following the economic changes of 1978. It has since seen substantial growth in population, economic expansion, and landscape change. The growing scope of Beijing's urban area has attracted significant attention [42–47]. Between 1949 and 2022, Beijing's population grew significantly. In 2002, the population was 14.23 million, and by 2022, it had grown to around 21.84 million. This rapid expansion has been fueled by urbanization, economic development, and migration [48].
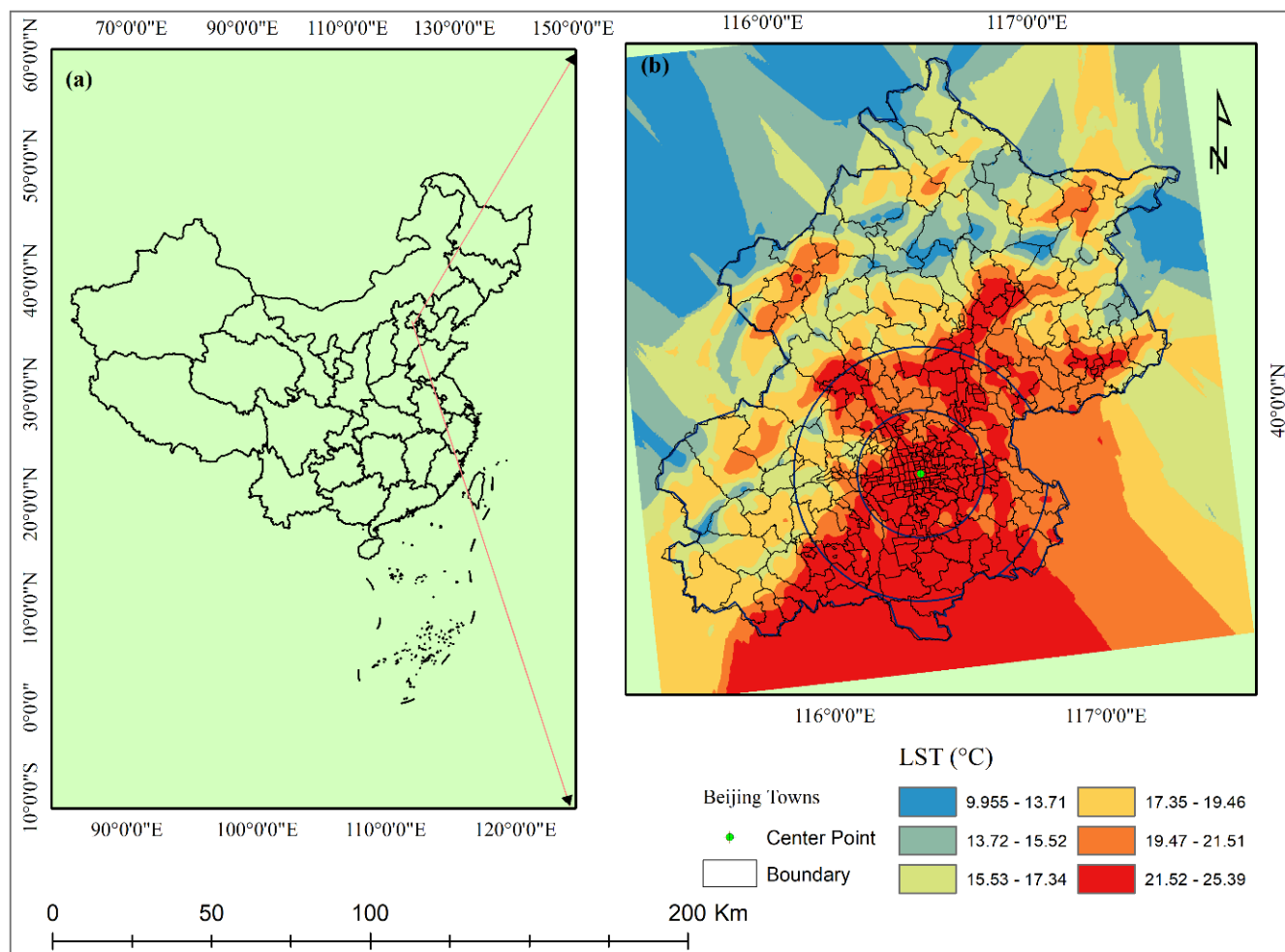
Figure 1. The location of the study area: (**a**) People's Republic of China (PRC), (**b**) Buffer zone divisions of Beijing Region with LST (2022).

1.2. Urbanization Levels

According to the Eleventh Five-Year Plan, Beijing is divided into four functional zones: the Core Functional Zone (Core zone, 94 km^2, 0.57%), the Urban Functional Extended Zone (Extended Zone, 1289 km^2, 7.77%), the New Urban Development Zone (NewDev-Zone, 6322 km^2, 38.12%), and the Ecological Conservation Zone (Eco-Zone, 8880 km^2, 53.54%). The Core Zone is used to develop political and cultural distinctions, the Extended Zone and the NewDev Zone focus on the development of commerce and manufacturing, respectively, and the EcoZone serves as a green ecological barrier and provides protection for water sources [49].

Zhang et al. [42] used ArcGIS 10.0 to create eight directional fans of land expansion radiating from the city center of Beijing. Buffer zones were created and overlayed with directional polygons. This analysis compares urban expansion in different directions and buffer zones across time. Beijing's urbanization hot zones were found to be within the 10 km to 20 km ranges.

Our buffer zone division, guided by Beijing's Eleventh Five-Year Plan, Beijing town boundaries, and Zhang's study, resulted in three distinct zones. For simplicity, the downtown boundary (core area) was approximated as a circular area with a 20 km radius. The transit area was defined as approximately within a range of 21–40 km, while the suburban area extended beyond 40 km, using proximity-based approximations. The buffer zone method was used to investigate the variation in urban-rural gradient and its connection to LST in more detail [50]. Using buffer zones allows for a more detailed investigation of LST

variations in newly developed urban areas and older urbanized regions [34]. This buffer zone technique helps policymakers target crucial places for mitigation and adaptation strategies, improving urban development efforts to reduce heat stress [13].

2. Materials and Methods

2.1. Datasets

We built our datasets according to the various literature reviews, availability of data, detecting multicollinearity, and categorizing determinants into theme groups to analyze their impact on the LST (Table 1). The dominant determinants affecting LST changes can be categorized into natural and human-induced variables [51].

Table 1. Datasets and sources.

Datasets	Time	Spatial Resolution	Sources
LST (K)		1000 M	NASA Earth Data (MOD11A1.006)
Emissivity		1000 M	
AOD		1000 M	NASA Earth Data (MCD19A2 v061)
Sensible heat flux		0.25 deg	NASA Earth Data (GLDAS_NOAH025)
NDVI	2002–2022	500 M	NASA Earth Data (MOD13A1 V6)
NDBI, NDWI		500 M	NASA Earth Data (MOD09GA)
Precipitation		0.1 deg	NASA Earth Data (GPM_3IMERGDL v06)
Albedo		500 M	NASA Earth Data (MCD43A1)
Nighttime light		30, 15 arcsec	Earth Observation Group (DMSP-OLS and VIIRS)
Population	2002–2020	30 arcsec	Worldpop.

Land cover indices are critical for understanding the LST of urban processes. Numerous indices, including the Normalized Difference Built-up Index (NDBI), Normalized Difference Water Index (NDWI), and Normalized Difference Vegetation Index (NDVI), serve as indicators of built-up areas, water presence, and vegetation, respectively [52], and population density and nighttime light both have a substantial impact on LST [53]. Furthermore, climate variables such as Surface Emissivity, Aerosol Optical Depth (AOD), Sensible Heat Flux, surface albedo, and precipitation are critical in understanding how heat retention and atmospheric conditions affect LST distribution in metropolitan areas [37,54,55]. Natural variables include land use indices (NDVI and NDWI), which reflect natural determinants and climate variables, whereas NDBI, population density, and nighttime light are human-induced variables.

2.1.1. Land Surface Temperature

This study used data from NASA Earth Data, a global platform that contains satellite observations from a variety of remote sensing missions and devices. The Terra and Aqua satellites use MODIS data to measure land surface temperature, indices of vegetation, and other environmental parameters. MOD11A1.061 Terra Land Surface Temperature and Emissivity Daily Global 1 km mean are annual products that we chose to cover the Beijing Region from 2002 to 2022 to investigate the effects of urban-induced land use change on land surface temperature, as shown in Figure 2. NDBI and NDWI variables were determined using Equations (2) and (3), respectively.

Several scientists used land surface temperature datasets from MODIS to assess the surface energy balance and study land surface temperature spatiotemporally [56]. Urbanization and Land Surface Temperature Dynamics [34,36,51,57–63]. Preprocessing of variables produced from MODIS datasets conducted using Equation (1):

Unit conversion of MOD11A1.061 data:

$$LST = DN \times 0.02 - 273.15 \qquad (1)$$

LST is the land surface temperature value (°C) and *DN* is the pixel grayscale value (K)

$$NDBI = (SWIR - NIR)/(SWIR + NIR) \tag{2}$$

$$NDWI = (NIR - SWIR)/(NIR + SWIR) \tag{3}$$

where *SWIR*—Short-wave infrared (sur_refl_b06), *NIR*—Near-infrared (sur_refl_b02).

The aggregation method is important for addressing the mixed-pixel issue. Aggregating maps at set spatial resolutions improves data consistency and eliminates inconsistencies resulting from mixed-pixel effects, hence increasing analytical reliability [64–67]. All data were aggregated, and the newly developed grided data were standardized utilizing Equation (4):

$$LST = (LST_i - \mu)/\sigma \tag{4}$$

where *LSTi* denotes total *LST* for the *i*th year, and σ and μ are the standard deviation and mean of the *LST* dataset, respectively. All the additional independent variables were standardized using the same methodologies.
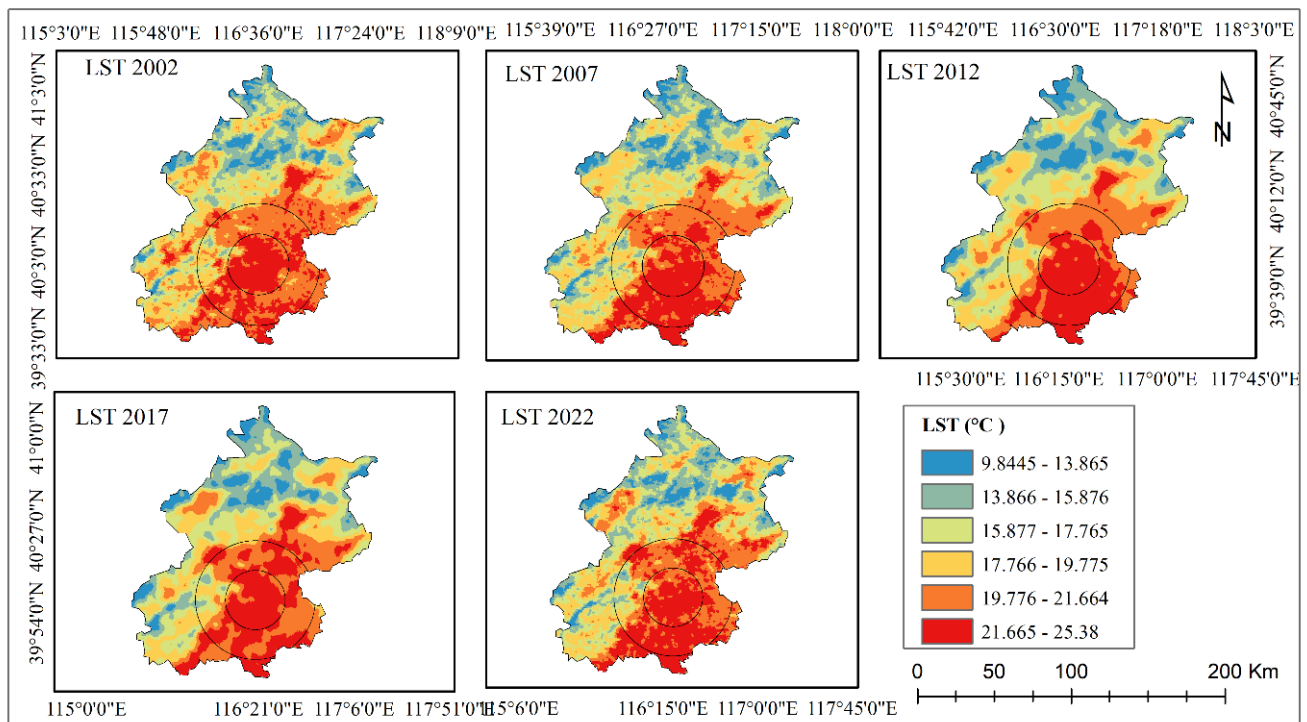

Figure 2. The land surface temperature.

2.1.2. Land Cover Data

The European Space Agency (ESA) Climate Change Initiative (CCI) provided land cover/use thematic map products from 1992 to 2022. Annual CCI-LC products with a spatial resolution of 300 m have been widely used as compelling data in LC-related investigations [68]. This dataset contains 22 global LC categories and uses the Food and Agricultural Organization of the United Nations land cover classification system [69]. The area proportion of forest loss and land cover transitions was calculated using the ESA CCI Land Cover datasets [70]. The study uses ESA CCI-LC records to investigate land-use intensity variations within and outside protected areas [71]. We then retrieved LULC from ESA for the Beijing Region in 2002, 2012, and 2022, as shown in Figure 3.
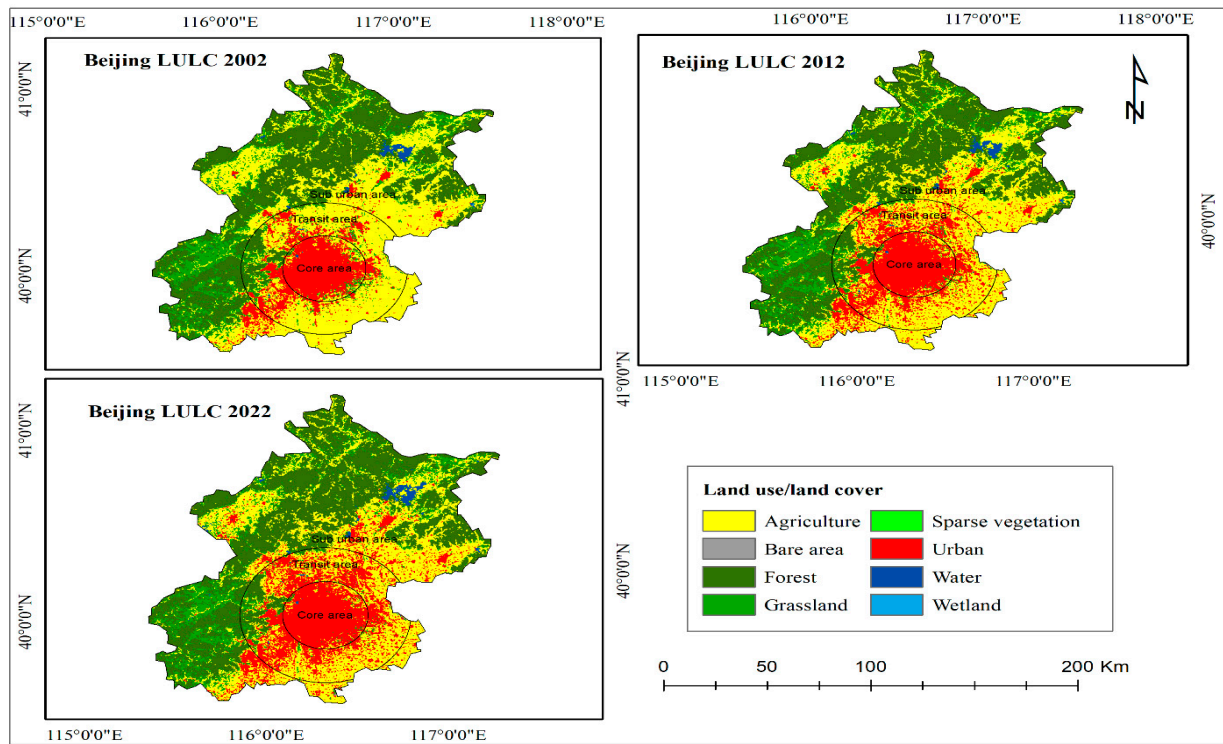
Figure 3. Land use land cover change.

2.2. Methods

Among the global models, we have chosen the Ordinary Least Squares (OLS) model, as well as the local model Geographically Weighted Regression (GWR), due to their interpretability and ability to provide direct coefficients. A combination of OLS and GWR models was used across three buffer zones (core, transit, and suburban areas). The study conducted a multitemporal analysis encompassing 2002, 2012, and 2022, thereby providing a better understanding of changes.

In OLS, important indicators consist of t-statistics and *p*-values for evaluating coefficient significance, Variance Inflation Factor (VIF) for determining multicollinearity (with VIF > 7.5, shows high level), Akaike Information Criterion (AIC) to measure model quality, and R-squared (R^2) to demonstrate the proportion of variance that the model explains. Adjusted R-squared simplifies this by taking into account the total number of predictors, which makes it useful for assessing models with several variables. The independent variables connected to the dependent variable were calculated using Equation (4).

$$Y_i = a_o + a_k X_i^k + e \tag{5}$$

where "*Y*" is the dependent variable, *LST*; *k*—variables, *i*—sample, a_o is the intercept; α_k is the coefficients; and *e* is the error/residuals.

GWR computes coefficients at each point, revealing how the direction and strength of variable impacts vary with space. The mean coefficient in GWR, a summary measure, represents the average impact of each independent variable across every location. The GWR equation for calculating independent variables and the dependent variable is given (6):

$$Y_i = a_{io}(u_i, v_i) + \sum_{k=1}^{n} a_{ik}(u_i, v_i) * X_i^k + \in_i \tag{6}$$

where (*ui, vi*) symbolizes the coordinates, *i*—sample, *k*—variable, a_{ik} (*ui, vi*) is the regression coefficient of each variable at point *i*, a_{io} (*ui, vi*) is a constant term, and $\in_i$ is the random error term at point *i*. n is the number of independent variables.

The R-squared and modified R-squared values of both models have been compared to determine the relative importance of the variables that are independent in generating LST changes.

3. Results

3.1. Overall Changes in Spatiotemporal LULC Across the Entire Period

For a better understanding of the LULC change, Table 2 and Figure 3 show the area coverage and changes, respectively. The results enable us to determine the extent to which area of change in LULC has occurred for each sort of LULC class during the last 20 years.

Table 2. Land use area coverage.

Land Use Classes	LULC 2002		LULC 2012		LULC 2022	
	Area (km^2)	Area (%)	Area (km^2)	Area (%)	Area (km^2)	Area (%)
Agriculture	6529.23	39.77	5933.42	36.14	5400.72	32.90
Bare area	0.91	0.01	0.34	0.002	0.64	0.004
Forest	5663.06	34.49	5690.53	34.66	5993.02	36.50
Grassland	2095.99	12.77	1920.80	11.70	1717.67	10.46
Sparse veg.	0.33	0.002	0.33	0.002	0.36	0.002
Urban	2008.09	12.23	2757.88	16.80	3156.28	19.23
Water	117.60	0.72	111.81	0.68	146.57	0.89
Wetland	2.18	0.013	2.28	0.014	2.14	0.013
Total	16,417.40	100.00	16,417.40	100.00	16,417.40	100.00

Urban areas changed the most, rising by 1148.19 km^2 (57.18%), thereby adding 19.225% to its entire area in 2002, as indicated in Tables 3 and 4. This area was largely converted from agricultural and grassland types of land use, and was rarely converted into other land-use types. Over the past two decades, agricultural land decreased by 1128.51 km^2 (17.284%), while grassland decreased by 378.33 km^2, being mostly converted to urban areas. The fast expansion of urban areas in the Beijing Region can be attributed to the region's quickly growing population, migration to urban areas, and the resulting infrastructure and institutional development.

Over the last two decades, forest area has expanded by 329.95 km^2 (5.826%). Expanding forest coverage regulates surface areas through evapotranspiration, shade, and raising albedo while decreasing urban heat-retaining, thereby moderating the rise in LST. In the entire study period, sparse vegetation and waterbody had a modest area of modification, as shown in Table 2 and Figure A2, compared to its 2002 area.

Table 3. Land use change.

Land Use Classes	Change (2002–2012)		Change (2012–2022)		Change (2002–2022)	
	Area (km^2)	% Change	Area (km^2)	% Change	Area (km^2)	% Change
Agriculture	−595.81	−9.13	−532.70	−8.98	−1128.51	−17.28
Bare area	−0.58	−62.90	0.30	88.29	−0.28	−30.15
Forest	27.47	0.49	302.48	5.32	329.95	5.83
Grassland	−175.19	−8.36	−203.13	−10.58	−378.33	−18.05
Sparse veg.	0.00	0.00	0.03	10.04	0.03	10.04
Urban	749.79	37.34	398.40	14.45	1148.19	57.18
Water	−5.79	−4.92	34.76	31.09	28.97	24.64
Wetland	0.10	4.67	−0.14	−6.29	−0.04	−1.92

Table 4. Land use transformation (areas, in Km^2).

	Land Use Classes	LULC 2022							
		Agriculture	Bare area	Forest	Grassland	Sparse veg.	Urban	Water	Wetland
LULC 2002	Agriculture	5286.82	0.149	151.90	88.93	0.04	988.12	29.50	0.08
	Bare area		0.11				0.80		
	Forest	31.67		5555.59	72.49		1.50	2.33	
	Grassland	77.35	0.46	284.92	1553.88		175.81	3.42	
	Sparse veg.	0.01				0.32			
	Urban	0.85	0.02	0.05	1.87		1989.27	0.15	
	Water	4.00		0.53	0.47		0.98	111.09	0.58
	Wetland	0.02		0.03	0.03		0.52	0.08	1.48

3.2. Temporal Change in LST Across LULC Types

The study found significant variations in land surface temperatures in Beijing between 2002 and 2022 across various land use classes. Urbanization drove the greatest increase, with bare areas along the time scale. Wetlands, forests, grassland, water, and agricultural land saw a considerable increase, as shown in Table 5 and Figure A3. Urban areas have higher temperatures due to impervious surfaces, industrial activities, and expansion of infrastructures, whereas bare areas have high temperatures due to minimal vegetation cover.

Table 5. The LST of different land use categories.

Land Use Types	Mean LST (°C), 2002	Mean LST (°C), 2012	Mean LST (°C), 2022	Change (2002–2022)
Agriculture	19.929	19.439	20.580	0.652
Bare area	20.145	20.544	20.961	0.816
Forest	16.295	16.592	16.581	0.286
Grassland	17.635	17.196	17.947	0.312
Sparse veg	16.598	16.760	17.287	0.690
Urban	21.370	21.603	22.274	0.904
Water	14.276	13.711	14.575	0.299
Wetland	18.056	17.380	18.267	0.211

On a time scale, forests' LST values show the lowest records throughout the study period. This result is best explained by forests' ability to decrease the amount of heat retained by the surface of the earth via transpiration. Expanding urban forests can serve as a natural climatic solution for mitigating the LST.

The LST values for the classifications of water bodies and wetlands increased over time. The environment around densely urbanized areas can elevate LST in nearby water bodies and wetland areas. Overall, the LST increased significantly across all LULC types.

3.3. Spatial-Temporal Variance in LST and LULC Changes Across Buffer Zones

The buffer area method was employed for separating the areas based on distance into three zones. The primary goal of using the buffer area method is to discover the variables that influence LST in the three zones.

The core area, due to its fast urbanization, which has a significant influence on impervious surfaces, suffered the biggest increase in LST (Table 6 and Figure A4). The proliferation of impermeable surfaces, such as asphalt and concrete, caused by urban growth has resulted in higher LST. This is demonstrated by a significant increase in LST in metropolitan areas, which rose by 0.904 °C between 2002 and 2022.

The transit area, too, experienced a 0.768 °C increase in LST between 2002 and 2022, owing to the substantial transition of agricultural and grassland areas to urban land. Forests, which had a modest (16.097 km^2) increase, have played a key role in buffering the impact of urbanization on LST. Forest cover grew, showing the cooling influence of forest areas relative to the core area. Table 6 and Figure A4 show that initiatives to restore and conserve forests can help decrease the LST impact of urbanization.

The suburban areas saw a slight LST increase of 0.248 °C (Table 6 and Figure A4) owing to a more balanced development pattern, with urban growth mitigated by increases in forest cover. The suburban area, which had less urbanization, benefited from increased forest cover, and this helped to mitigate the rise in LST. This demonstrates that protecting and developing forest areas in suburban areas is a potential approach to reducing the warming impacts caused by urbanization. Difference in LST across buffer zones proves the need for spatially focused land use alternatives that account for each region's unique characteristics.

Table 6. Land use and LST change in buffer zones (areas, in Km^2).

Land Use Classes	Year	Core Area	Transit Area	Sub Urban Area
Urban	2002	1030.40	697.72	279.98
	2012	1108.85	1161.36	487.57
	2022	1135.37	1384.49	633.92
	change 2002–2022	104.97	686.77	353.94

Table 6. *Cont.*

Land Use Classes	Year	Core Area	Transit Area	Sub Urban Area
Agriculture	2002	153.30	2317.68	4058.26
	2012	113.20	1931.92	3888.30
	2022	93.62	1720.68	3586.42
	change 2002–2022	−59.68	−597.00	−471.84
Grassland	2002	63.16	263.05	1769.79
	2012	25.29	187.05	1708.46
	2022	18.23	157.71	1541.73
	change 2002–2022	−44.93	−105.34	−228.06
Forest	2002	7.04	290.22	5365.62
	2012	6.80	289.41	5394.32
	2022	7.22	306.32	5679.29
	change 2002–2022	0.18	16.10	313.67
Bare area	2002		0.914	
	2012		0.339	
	2022		0.643	
	change 2002–2022	0	−0.271	
Sparse Veg	2002			0.330
	2012			0.330
	2022			0.363
	change 2002–2022			0.033
Water	2002	2.551	6.479	108.57
	2012	2.488	6.451	102.87
	2022	2.378	6.335	137.86
	change 2002–2022	−0.173	−0.144	29.29
Wetland	2002		1.049	1.121
	2012		0.579	1.702
	2022		0.585	1.553
	change 2002–2022	0	−0.464	0.432
Mean LST, (°C)	2002	21.537	17.616	17.616
	2007	21.962	17.646	17.646
	2012	20.467	20.600	17.679
	2017	20.557	20.956	17.835
	2022	22.441	21.235	17.863
	change 2002–2022	0.904	0.768	0.248

3.4. Performance Determines the Driving Variables for LST in the Buffer Zones

Complete statistics include OLS and GWR summaries as well as model diagnostics for 2002, 2012, and 2022 over three buffer zones (core, transit, and suburban areas). These provide a range of statistics, including coefficients, t-statistics, probabilities, VIFs (Tables A1–A3), and R-squared values, which are essential for evaluating the interactions between variables over time. The study employed OLS and GWR to investigate the connection between LST and variables in three buffer zones in 2002, 2012, and 2022.

The OLS regression findings across all buffer zones demonstrated comparable model behavior; overall values for R-squared ranged from 0.708 to 0.821 (Table 7). The Koenker's (BP) statistic was found to be insignificant ($p > 0.01$) for the entire period and buffer zones, indicating that the model is consistent. Similarly, the Jarque–Bera statistic was calculated and shown to be statistically insignificant ($p > 0.01$) throughout all scenarios, implying that residuals have a Gaussian distribution. The values of the VIF of the auxiliary variables have been calculated employing a threshold smaller than 7.5 (Tables A1–A3), demonstrating no multicollinearity among the auxiliary variables. The coefficients of NDBI, nighttime light, population, precipitation, and sensible heat flux were all positively related, whereas NDVI and NDWI were inversely related to LST. However, surface albedo and surface emissivity were positively related in the core and transit areas but negatively correlated in the suburban area. The computed coefficients in the OLS model show that increasing all variables in the study area enables the increasing intensity of LST. Conversely, NDVI and NDWI can reduce and mitigate LST.

Table 7. OLS Diagnostics: Model Variables.

Performance Indicators	2002			2012			2022		
	Core	Transit	Suburban	Core	Transit	Suburban	Core	Transit	Suburban
AICc [d]:	5315.32	5251.867	9170.650	8984.047	7844.015	6951.490	4999.604	5557.587	4831.840
Multiple R-Squared [d]:	0.709	0.732	0.721	0.708	0.803	0.812	0.709	0.818	0.821
Adjusted R-Squared [d]:	0.708	0.731	0.720	0.707	0.802	0.811	0.708	0.817	0.820
Global Moran's I:	0.707	0.659	0.565	0.751	0.645	0.486	0.709	0.626	0.392
Joint F-Statistic [e]:	929.616	669.572	257.381	1027.806	1151.875	885.656	652.537	1017.371	713.363
Joint Wald Statistic [e]:	8028.359	4135.984	1923.575	6609.348	8671.371	9514.314	5255.040	7171.393	6102.421
Koenker (BP) Statistic [f]:	369.102	236.751	493.996	426.881	250.110	67.783	126.081	131.173	147.663
Jarque–Bera Statistic [g]:	246.842	380.982	741.799	113.628	126.883	121.214	71.335	135.857	145.782

[d] Akaike's Information Criterion (AICc) and R-squared measures model fit and performance. [e] If the Koenker (BP) Statistic [f] is statistically significant, utilize the Wald Statistic to evaluate overall model significance. [f] Koenker (BP): A statistically significant test ($p < 0.01$) indicates that the hypothesized relationships are inconsistent. [g] Jarque–Bera A statistically significant test ($p < 0.01$) indicates that model predictions are biased (residues are not regularly distributed).

GWR (Table 8) indicated variation in the spatial distribution in the LST relationships. The GWR model's lower AICc, higher R-squared, and adjusted R-squared, as well as the Moran's I of StdResid approaches zero compared to the OLS model results, show that it can better describe the spatial connection among LST and its impacting variables than the global OLS model. GWR's ability to account for local variations, mainly those driven by rapid urbanization or land use changes, improved between 2002 and 2022. The GWR model's lower AICc, higher R-squared, and adjusted R-squared values indicate a better fit and improve comprehension of variable interactions across geographical areas [72–75].

Despite the OLS model, the geographical distributions of local R2 for the GWR models demonstrated regional differentiation, with the highest indication representing the predictive power for LST in the core and transit areas over two decades (Figure 4). Higher R^2 values were seen in core and transit zones, where the correlation between rising LST and impacting variables was well established. This shows that both increased and diminished impacting variables are the principal drivers of LST changes. Between 2002 and 2022, the Northeast part of Beijing's suburban areas gradually developed, and these variables had a significant impact on the LST, resulting in more power and consistency over the two decades. This improved match shows that the variables driving LST change are now easier to identify. The model performance in Beijing's southeast is somewhat below average, which could indicate that new causes or environmental factors have impacted this area.

Table 8. GWR Diagnostics: Model Variables.

Performance Indicators	2002			2012			2022		
	Core	Transit	Suburban	Core	Transit	Suburban	Core	Transit	Suburban
Bandwidth:	2957.0	2466.0	275.0	1974.0	2837.0	2060.0	2684.0	2254.0	1098.0
Residual squares:	1028.92	1193.58	3186.05	2017.82	2604.06	3450.65	996.35	1506.20	1919.85
ENP:	20.01	19.51	224.42	58.60	19.32	19.53	19.69	20.59	35.20
AICc:	5314.68	5251.28	7789.53	8981.70	7842.69	6950.90	4999.60	5556.75	4833.22
R-squared:	0.721	0.764	0.789	0.733	0.824	0.843	0.761	0.850	0.840
Adjusted R-squared:	0.709	0.731	0.767	0.719	0.812	0.831	0.759	0.838	0.826
Global Moran's I:	0.359	0.341	0.254	0.225	0.323	0.241	0.273	0.269	0.231

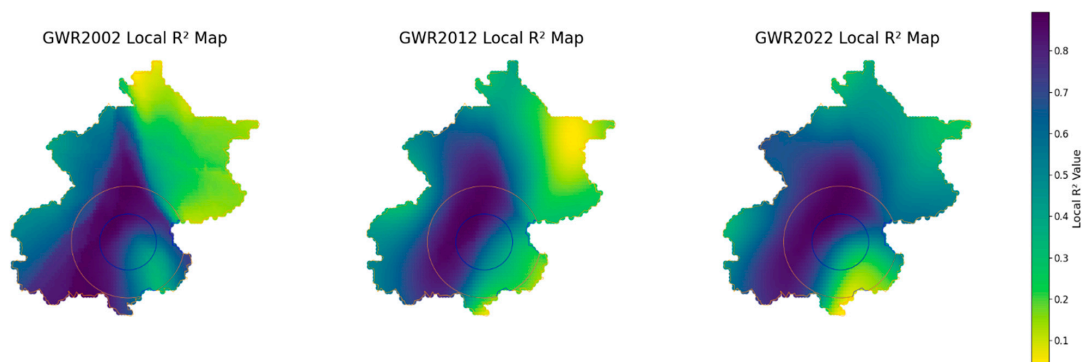ENP denotes the Effective Number of Parameters.

Figure 4. Local R^2 values of GWR.

3.5. Evaluation of Significant Variables Influencing LST

Table 9 and Figure A1 indicate the spatiotemporal distribution and relationship of latent and observed variables' mean coefficients and LST using GWR model results from 2002 to 2022.

Table 9. GWR summary—mean coefficient of independent variables.

	2002			2012			2022		
	Core	**Transit**	**Suburban**	**Core**	**Transit**	**Suburban**	**Core**	**Transit**	**Suburban**
Factors	Mean Coef.	Mean Coef.	Mean Coef.	Mean Coef.	Mean Coef.	Mean Coef.	Mean Coef.	Mean Coef.	Mean Coef.
Intercept:	93.31	71.05	5.99	32.63	43.32	6.10	61.92	50.27	7.46
NDBI:	24.42	18.60	16.07	26.58	18.94	14.96	27.75	24.65	11.43
NDVI:	−14.11	−11.03	−8.58	−14.53	−14.03	−7.17	−16.32	−13.05	−4.82
NDWI:	−13.57	−10.03	−8.40	−15.14	−11.62	−11.79	−16.94	−10.07	−7.65
Nighttime light:	0.39	0.31	0.06	0.81	0.48	0.04	0.95	0.46	0.08
Population:	0.09	0.06	0.001	0.09	0.01	0.01	0.11	0.08	0.02
Precipitation:	0.98	0.35	1.13	0.57	0.48	3.14	0.61	1.49	3.71
Sensible heat flux:	0.04	0.01	0.03	0.08	0.03	0.02	0.39	0.14	0.004
Surface albedo:	0.06	0.34	−0.58	0.03	0.23	−0.35	0.01	0.07	−0.67
AOD:	0.12	0.09	0.03	0.82	0.06	0.003	0.03	0.04	0.60
Surface emissivity:	4.61	2.94	−5.83	6.52	3.91	−9.287	6.87	3.12	−11.21

The mean coefficient of NDVI declined from −14.11 (2002) to −16.32 (2022) in the core and −11.03 (2002) to −13.05 (2022) in transit areas (Table 9 and Figure A1), indicating lesser vegetation density, whereas higher values in suburban areas imply more forest cover. This distribution demonstrates that areas with low NDVI correspond to higher LST because artificial impermeable surfaces absorb more heat. Conversely, places with higher NDVI have lower LST due to the cooling effect of vegetation. The mean coefficient values of surface emissivity were higher in core and transit areas, resulting in increased heat retention and radiation, intensifying LST. The increased frequency of impermeable surfaces, combined with high emissivity, is expected to contribute to heat accumulation in core and transit zones, resulting in considerable LST variations.

The temporal and spatial distribution of AOD over the last two decades indicates a lowering trend of mean coefficient, 0.12 (2002) to 0.03 (2022) and 0.09 (2002) to 0.04 (2022), in Beijing's core and transit zones, respectively, but a minor rise, 0.03 (2002) to 0.60 (2022), in suburban areas, as shown in Table 9 and Figure A1. This decrease in AOD in the core and transit areas is mostly due to the relocating of heavy and polluting companies to less densely populated nearby regions, specifically Hebei Province and Tianjin, as part of the Air Pollution Prevention and Control Action Plan (2013–2017). In contrast, suburban areas have seen a minor increase in AOD, most likely due to pollution blowing in from adjacent places such as Hebei and Tianjin, where pollutants from heavy and polluting companies can be transported into Beijing by regional wind patterns, thereby affecting the LST.

The NDWI mean coefficient trend has been increasing in suburban areas over the last two decades (Table 9 and Figure A1), indicating slight water and soil moisture conservation, while Beijing's core and transit areas have decreased, pointing out that urbanization's influence on vegetation and water retention has reduced surface moisture content and contributed to an increase in LST. The mean coefficient of surface albedo has increased in suburban areas, indicating a favorable shift toward more reflecting surfaces, potentially due to a rise in forest cover or land-use modifications. In contrast, the minor decrease in albedo in the southeast areas of Beijing's core and transit areas could indicate ongoing urbanization and contribute to LST rises. Precipitation shows positive coefficient values throughout the last two decades. The mean positive coefficient values of precipitation are associated with increased LST in core and transit areas due to impermeable surfaces, limiting efficient cooling through soil moisture, evapotranspiration, and water absorption.

The mean coefficient of sensible heat flux increases dramatically in the core and transit area, from 0.04 (2012) to 0.39 (2022) and 0.01 (2002) to 0.14 (2022), respectively, as shown in Table 9 and Figure A1. Impervious surfaces in core and transit areas absorb and hold heat,

slowly releasing it and increasing LST. In contrast, the low mean coefficient in a suburban region shows that permeable surfaces and forest cover are more effective at LST dissipation.

Human-induced variables, as shown in Table 9 and Figure A1, such as population density, NTL, and NDBI, have a positive connection with LST in the core and transit areas but a lower positive coefficient correlation in suburban areas. The population's mean coefficient values increased from 0.09 (2002) to 0.11 (2022) and 0.06 (2002) to 0.08 (2022), as indicated in Table 9 and Figure A1, over two decades in the core and transit areas, demonstrating an increasing concentration of people. Still, a decreasing mean coefficient was observed in the suburban areas, showing that there might be a migration of people from the suburban to core areas. This increased population density increases energy demand in the form of more air conditioners, vehicles, and buildings, which directly elevates LST. The concentration of people and activity in core and transit regions aggravates these effects, especially during peak energy demand days. From 2002 to 2022, the mean coefficient of nighttime light and its spatial distribution in core and transit areas rose as a result of energy consumption and artificial lighting, contributing to the LST trend. Suburban areas have smaller facilities and fewer people, resulting in lower nighttime light. The increase in nighttime light and population density over the last two decades coincides with the rapid growth of the NDBI, indicating increasing urbanization.

4. Discussion

This analysis combines two decades of remote sensing data and a buffer zone technique to demonstrate how the potential driving variables in core-transit-suburban areas influence LST patterns. The key driving variables were identified, and the spatial-temporal relationship between LST and driving variables was investigated using a spatial regression model, as shown in Table 9 and Figure A1.

The core area, which is characterized by dense urbanization, experienced the greatest LST increase during the research period, with a 0.904 °C rise from 2002 to 2022 (Table 6). Human-induced variables like NDBI, population density, and nighttime light mostly cause this large warming. The positive mean coefficient between NDBI and LST (Table 9 and Figure A1) emphasizes the importance of built-up density in enhancing heat absorption. The removal of vegetation with impervious surfaces inhibits natural cooling mechanisms, exacerbating the LST impact. Increased nighttime light represents increased human-induced activity, which contributes to LST through energy use. Furthermore, population development in the core area raises energy consumption, vehicle emissions, and heat-generating activities, worsening LST. Hence, the human-induced variables intensified heat accumulation in the core area. Natural variables also play a role; low NDVI, surface albedo, surface emissivity, and NDWI imply a loss of vegetation and water bodies, reducing evapotranspiration and heat mitigation capabilities. Furthermore, high sensible heat flux values in urban surfaces increase the absorption of heat, which accelerates the warming trend. These studies highlight the significant role of urbanization in driving LST in the core area, which is consistent with current worries about the development of LST due to the rapid development of urban areas. The findings demonstrate a large increase in LST values in metropolitan areas as the natural landscape transitions to impermeable surfaces [76,77]. According to Gupta and Aithal [78], by 2050, Asia and Africa will account for approximately 90% of global urbanization, resulting in major temperature increases.

The transit area, which serves as the divide across the core and suburban areas, experienced a moderate LST rise of 0.768 °C (Table 6) during the research period. Urban development spillover plays a crucial role here, as the rise of urban communities boosts built-up areas while demonstrating less density than in the core. Modest NDBI and nighttime light values indicate this change (Table 9 and Figure A1), showing expanding urban outskirts and localized warming impacts. Population density and sensible heat flux in this area also add to higher heat outputs and lead to a rise in LST. In regard to natural variable aspects, NDVI, surface albedo, and NDWI values indicate the existence of fractured agricultural areas and areas that have vegetation cover, which give certain cooling

benefits. Nevertheless, continuous development in the transit zone gradually eliminates these ecological buffers. These variations illustrate the twin stresses of human-induced and natural variable changes in the transit zone, which interact with rising manmade pressures. Studies show that urbanization has led to a rise in the world's average LST by 0.26–0.34 °C every decade [79].

The suburban areas, with their smallest LST rise of 0.248 °C (Table 6), take advantage of their natural surroundings but are nevertheless subject to growing problems. Natural variables take prominence here, with greater NDVI, surface albedo, and NDWI values contributing to lower LST via increased evapotranspiration and soil moisture, allowing natural ecosystems to maintain thermal balance. However, continued urban expansion and agricultural and grasslands being diminished (Table 6) are gradually lessening the natural cooling impacts. Precipitation variability, together with rising aerosol optical depth (AOD), affects regional cooling and warming patterns, as shown in Figure A1. Aerosols could encourage the development of clouds, but they also retain heat in the atmosphere, adding to regional warming. Rising LST in the core and transit areas, if not managed properly, will continue to have an impact on suburban areas, leading to local climatic instability and global warming. Forest area coverage shows increasing trends in Table 6 due to the Beijing Plain Area Afforestation Programme (BPAP), which was launched in 2012 to help reduce LST through increased forest cover, which cools the land via evapotranspiration, shade, and reduced heat absorption by soil and building surfaces [80]. Several experts stated that green spaces in urban development can help reduce heat absorption and promote ecologically sustainable land use [17,81].

Through the findings of spatial regression analysis, we determined that the combined influence of human-induced and natural variables had a considerable impact on the LST throughout the core, transit, and suburban areas. A comparison of the OLS and GWR models revealed that GWR performed better at representing the geographical variability of these variables. Furthermore, Moran's I statistics for residuals showed that the GWR model had less spatial autocorrelation than the OLS model, indicating that it was better suited to dealing with localized changes (Tables 7 and 8). Employing GWR, we created a spatiotemporal distribution of the human-induced and natural variables, revealing the key variables influencing LST across each buffer zone (Figure A1).

We found that Beijing has adopted an afforestation policy to mitigate and balance LST caused by urbanization in urban areas by reforestation in mountainous areas (suburban areas). From 2002 to 2022, LST climbed dramatically in the core (0.904 °C) and transit areas (0.768 °C), whereas suburban areas experienced a more modest rise of 0.248 °C. The transit area (686.77 km^2) experienced the most urbanization, followed by the suburban area (353.94 km^2) and the core (104.97 km^2). Forest coverage increased significantly in the suburban area, reaching 313.76 km^2, compared to 16.10 km^2 in the transit area and 0.18 km^2 in the core area (Table 6). This indicates how afforestation in mountainous suburban areas has alleviated some of the urbanization-induced LST consequences observed in other areas. According to this conclusion, the local government has established an afforestation policy, but it has not been adequate to entirely alleviate the rise in LST. Two key strategies should be considered to mitigate the LST effects. The first is implementing widespread tree-planting initiatives in suburban areas to enhance green cover and contribute to temperature regulation. The second involves adopting cooling measures directly within the core (downtown) areas. We have incorporated the following special recommendations based on our suggestions to address these strategies comprehensively: First, cooling methods should be employed to form buffer zones around the metropolitan core and transit areas. Furthermore, to limit heat absorption and radiation, the use of low-emissivity materials in construction and reflective pavements should be encouraged. Developing green belts in suburban areas can assist in absorbing heat from urban cores. Finally, encouraging suburban-to-core water redistribution can help with cooling efforts and improve climate comfort.

5. Conclusions

Beijing Region was chosen as a key case study to investigate how urbanization-induced changes in LULC affect LST. Focusing on the primary issue of LST and its contributing variables helps us to understand how variables influence LST throughout buffer zones—core, transit, and suburban. This technique is crucial for identifying and prioritizing essential variables in each zone, enabling more targeted efforts to reduce LST rise. The findings are as follows:

The buffer zone approach results demonstrate that the Beijing Region's LST climbed from 2002 to 2022, with increases of 0.904, 0.768, and 0.248 °C in core, transit, and suburban areas, respectively. The study shows that human-induced variables, such as NDBI, population density, and nighttime light, have significantly increased energy demand, resulting in more LST from air conditioners, vehicles, buildings, and artificial lighting in core and transit areas. In contrast, suburban areas have experienced slower growth due to less construction and forest cover preservation. Natural variables in suburban areas, such as NDVI, NDWI, emissivity, precipitation, and surface albedo, dominated and helped to reduce LST by regulating regional temperatures and increasing surface moisture content and evapotranspiration, thereby mitigating the warming effects of urbanization. In contrast, suburban areas have observed a slight increase in AOD, probably due to pollution blowing in from nearby regions, where pollutants from heavy and polluting industries can be brought into Beijing by regional wind patterns.

The spatiotemporal distribution of the human-induced and natural variables and their relationship with the LST, conducted based on the global (OLS) and local (GWR) models, could effectively detect the potential driving effects of the variables. The study's findings propose numerous solutions for improving LST in the three buffer zones, such as cooling methods, use of low-emissivity materials, developing green belts, and encouraging suburban-to-core area water redistribution.

Overall, this study illustrates how human-induced and natural variables affect LST in three buffer zones. Further research linking the findings of this study to the reasons for LST changes will be extremely beneficial in understanding and foreseeing future sustainable urban development and eco-friendly infrastructures in mitigating rising LST.

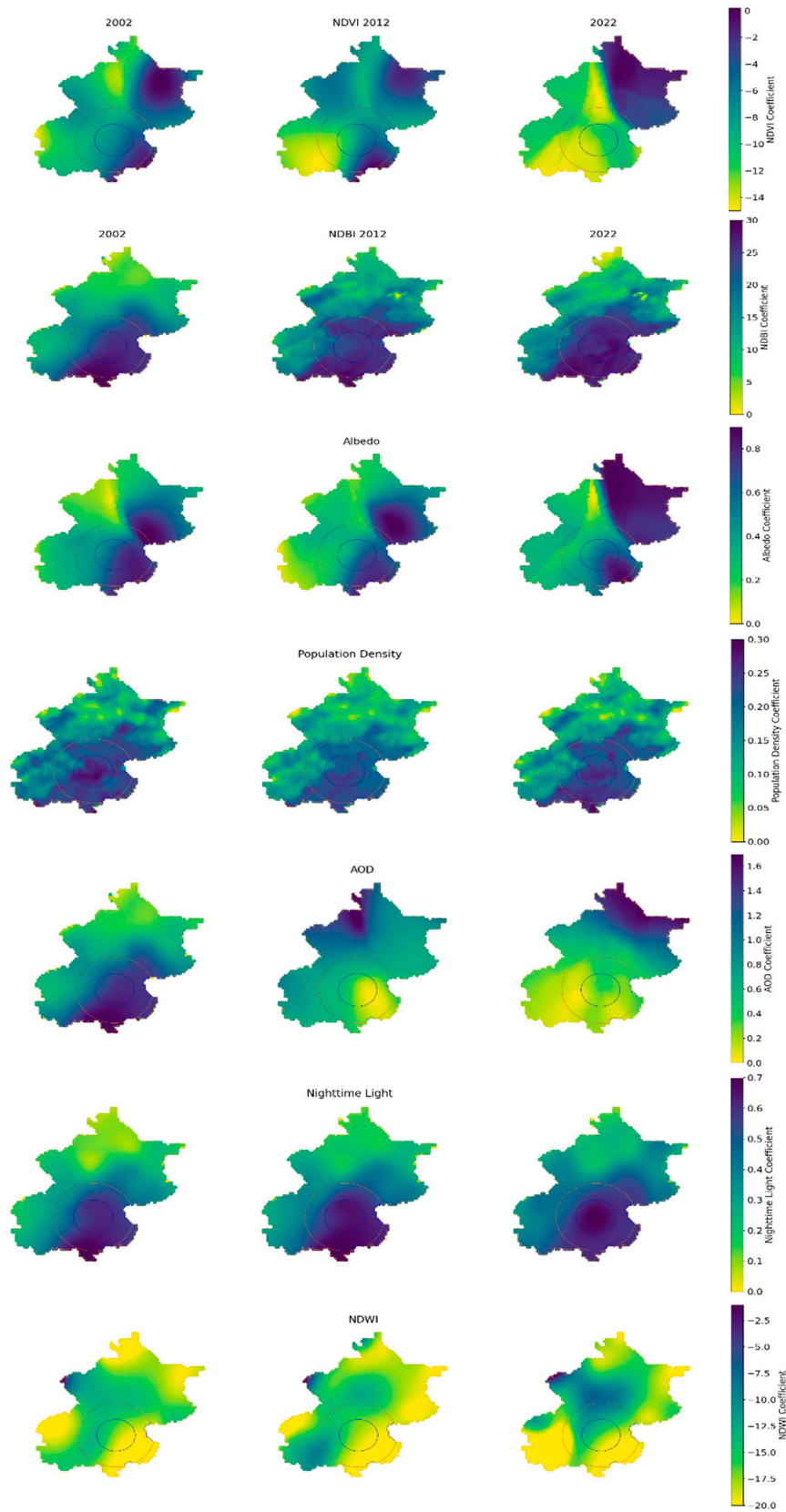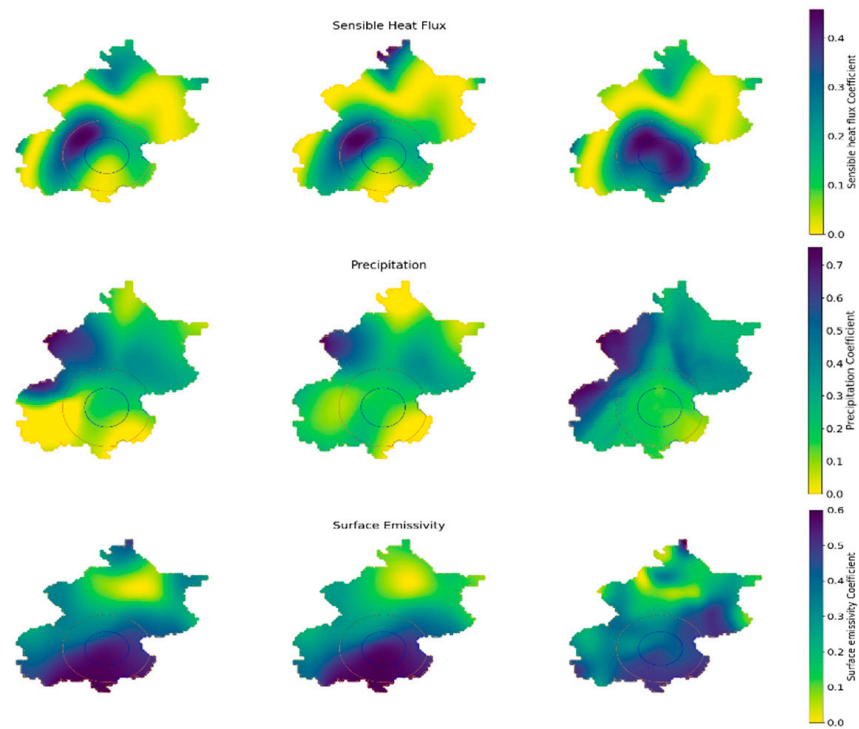# Appendix A

Figure A1. *Cont.*

Figure A1. Spatiotemporal changes in the determinant variables of local coefficients produced by the GWR mode.
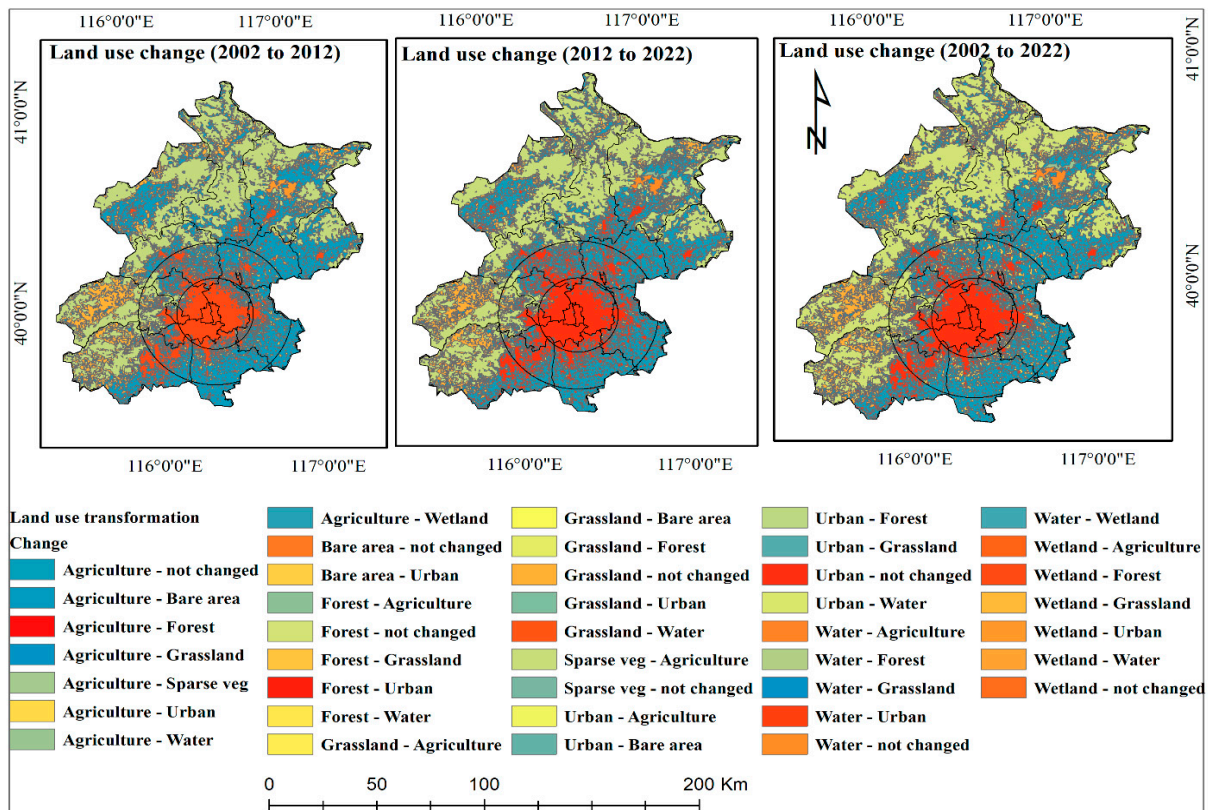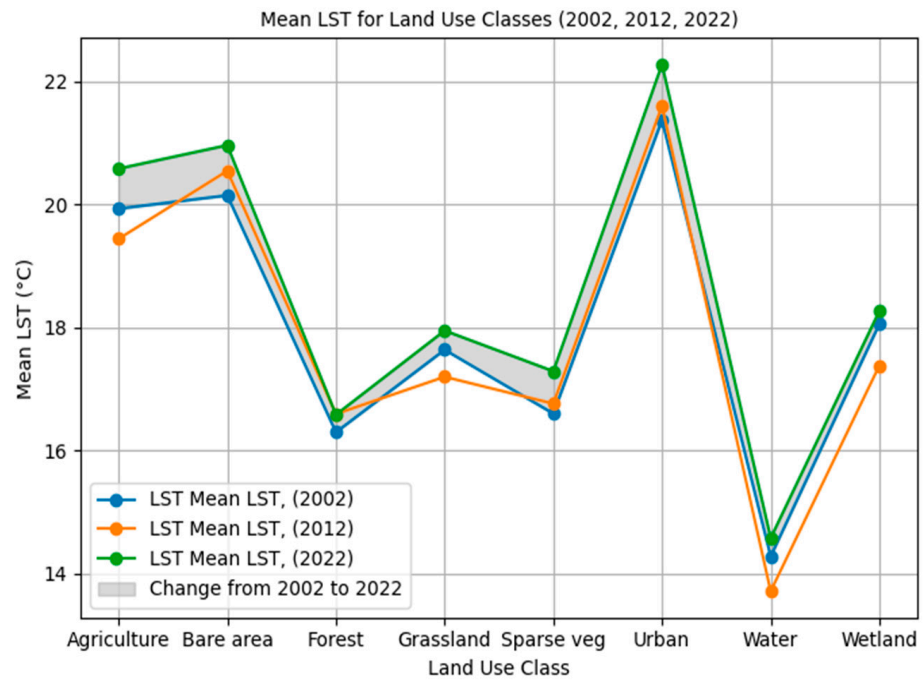

Figure A2. Land use transition dynamics.

Figure A3. Temporal changes of LST across land use classes.
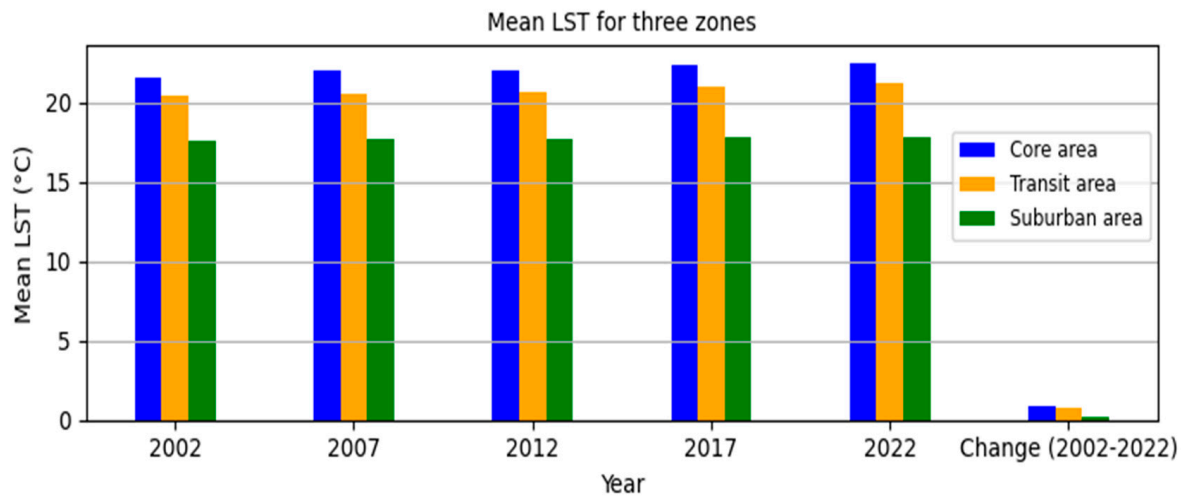

Figure A4. Temporal changes of LST variations in the buffer zones.

Table A1. OLS summary—coefficient, t-statistics, probability, robust_SE, and VIF of 2002.

Variable	Coefficient [a]			t-Statistic			Probability [b]			Robust_SE			VIF [c]		
	Core	Transit	Suburban	Core	Transit	Suburban	Core	Transit	Suburban	Core	Transit	Suburban	Core	Transit	Suburban
Intercept	93.536	49.854	21.760	30.619	11.399	5.421	0.000000 *	0.0695	0.000000 *	3.7690	5.5142	0.9856	-----	-----	------
Surface Albedo	2.045	0.076	−0.020	8.371	2.816	−2.101	0.000000 *	0.000000 *	0.035765 *	0.067	0.045	0.011	3.182	3.495	3.237
AOD	1.879	0.942	0.143	9.201	14.033	8.428	0.000000 *	0.000000 *	0.000000 *	0.101	0.791	0.688	3.361	3.136	3.137
Emissivity	41.99	27.01	−0.089	36.258	6.927	−6.359	0.000000 *	0.000000 *	0.000000 *	14.280	23.475	0.063	2.331	2.777	3.207
NDBI	18.662	16.150	8.490	27.73	19.689	4.858	0.000000 *	0.000000 *	0.000002 *	0.806	0.905	2.568	1.871	1.910	1.963
NDVI	−22.866	−10.863	−8.527	−21.240	−15.17	−1.196	0.000000 *	0.000000 *	0.000000 *	0.483	0.672	1.619	3.723	3.024	3.282
NDWI	−16.106	−15.922	−11.693	−22.421	−13.45	−10.81	0.000000 *	0.000000 *	0.000000 *	0.801	1.021	2.360	3.001	4.557	3.161
Nighttime light	0.411	0.297	0.054	3.482	2.977	1.633	0.000000 *	0.000000 *	0.000000 *	0.293	0.152	0.075	2.507	3.344	2.130
Population	0.020	0.080	0.025	4.822	2.104	0.259	0.000000 *	0.000000 *	0.001149 *	0.102	0.070	0.008	1.742	1.394	1.566
Precipitation	1.136	0.318	0.051	4.958	1.612	3.716	0.00021 *	0.1071	0.0002 *	0.225	0.178	0.034	2.132	2.709	1.195
sensible heat flux	0.038	0.039	0.021	8.718	4.078	2.135	0.000000 *	0.000000 *	0.032883 *	0.008	0.005	0.011	3.939	3.851	2.534

* A sign next to a number represents a statistically significant *p*-value (*p* < 0.01). [a] The coefficient indicates the intensity and type of association between the dependent variable and each explanatory variable. [b] Probability and Robust Probability (Robust_Pr): An asterisk (*) indicates a statistically significant coefficient (*p* < 0.01). [c] Variance Inflation Factor (VIF): Values greater than 7.5 imply duplication in explanatory variables.

Table A2. OLS summary—coefficient, t-statistics, probability, robust_SE, and VIF of 2012.

Variable	Coefficient [a]			t-Statistic			Probability [b]			Robust_SE			VIF [c]		
	Core	Transit	Suburban	Core	Transit	Suburban	Core	Transit	Suburban	Core	Transit	Suburban	Core	Transit	Suburban
Intercept	37.160	42.638	4.436	18.469	11.387	0.407	0.000000 *	0.000000 *	0.683916	2.185	3.980	12.960	------	------	--------
Surface Albedo	2.009	0.596	−0.342	41.152	12.477	−5.510	0.000000 *	0.000000 *	0.000000 *	0.055	0.054	0.071	3.560	3.356	2.926
AOD	0.011	0.011	0.026	19.356	12.949	35.651	0.000000 *	0.000000 *	0.000000 *	0.001	0.001	0.001	2.232	3.924	3.582
Emissivity	16.875	11.314	−9.809	27.216	7.540	−1.373	0.000000 *	0.000000 *	0.169987	7.522	16.808	52.948	2.322	1.764	1.394
NDBI	27.176	18.867	15.020	32.061	14.619	11.727	0.000000 *	0.000000 *	0.000000 *	0.626	1.115	1.458	2.667	2.164	1.744
NDVI	−7.215	−14.529	−13.886	−21.317	−18.688	−12.033	0.000000 *	0.000000 *	0.000000 *	0.378	0.577	0.926	3.131	3.993	3.551
NDWI	−17.003	−7.422	−11.858	−24.251	−7.685	−10.996	0.000000 *	0.000000 *	0.000000 *	0.777	1.039	1.905	3.667	3.567	2.682
Nighttime light	0.118	0.022	0.039	7.529	0.764	1.391	0.000000 *	0.000000 *	0.164358	0.168	0.037	0.025	1.907	1.548	2.040
Population	0.090	0.010	0.020	6.322	1.703	0.044	0.000000 *	0.088761	0.964687	0.101	0.104	0.003	1.814	1.309	1.730
Precipitation	2.988	0.459	0.552	18.531	3.583	3.476	0.000000 *	0.000360 *	0.000534 *	0.146	0.116	0.162	2.616	1.802	1.733
sensible heat flux	0.738	0.252	0.222	15.687	5.619	2.815	0.000000 *	0.000000 *	0.4928 *	0.520	0.491	0.915	3.480	3.260	1.604

* A sign next to a number represents a statistically significant *p*-value (*p* < 0.01). [a] The coefficient indicates the intensity and type of association between the dependent variable and each explanatory variable. [b] Probability and Robust Probability (Robust_Pr): An asterisk (*) indicates a statistically significant coefficient (*p* < 0.01). [c] Variance Inflation Factor (VIF): Values greater than 7.5 imply duplication in explanatory variables.

Table A3. OLS summary—coefficient, t-statistics, probability, robust_SE, and VIF of 2022.

Variable	Coefficient [a]			t-Statistic			Probability [b]			Robust_SE			VIF [c]		
	Core	Transit	Suburban	Core	Transit	Suburban	Core	Transit	Suburban	Core	Transit	Suburban	Core	Transit	Suburban
Intercept	62.490	50.044	5.148	27.074	14.154	0.481	0.000000 *	0.000000 *	0.630452	2.252	3.714	12.407	------	------	------
Surface Albedo	1.469	0.665	−0.426	18.998	12.963	−7.840	0.000000 *	0.000000 *	0.000000 *	0.079	0.056	0.062	2.543	3.007	2.568
AOD	0.601	0.287	0.043	5.150	22.727	41.182	0.000001 *	0.000000 *	0.000000 *	0.001	0.128	0.118	2.442	3.613	3.017
Emissivity	22.07	15.57	−6.890	33.306	11.315	−1.561	0.000000 *	0.000000 *	0.118689	8.093	15.492	50.077	2.279	1.676	1.396
NDBI	29.606	14.741	11.350	35.114	18.413	11.952	0.000000 *	0.000000 *	0.000001 *	0.675	1.065	1.657	2.537	2.617	1.436
NDVI	−6.654	−11.483	−8.656	−19.779	−14.78	−13.893	0.000000 *	0.000000 *	0.000001 *	0.391	0.477	1.095	3.012	4.174	3.462
NDWI	−8.361	−6.861	−6.358	−11.058	−9.691	−1.384	0.000000 *	0.000000 *	0.000001 *	0.659	0.966	1.250	2.571	4.941	2.386
Nighttime light	0.731	0.508	0.460	6.174	2.312	0.592	0.000000 *	0.020865 *	0.553736	0.001	0.003	0.013	1.893	1.980	1.679
Population	0.011	0.030	0.012	9.580	2.544	0.441	0.000000 *	0.068401	0.659558	0.000	0.040	0.030	1.716	1.360	1.446
Precipitation	0.708	1.495	−0.004	5.132	3.436	0.030	0.000001 *	0.000000 *	0.976285	0.140	0.100	0.138	3.510	3.187	1.925
sensible heat flux	0.038	0.005	−0.034	8.261	1.275	0.197	0.000000 *	0.000034 *	0.202559	0.005	0.004	0.009	3.743	3.608	1.670

* A sign next to a number represents a statistically significant *p*-value (*p* < 0.01). [a] The coefficient indicates the intensity and type of association between the dependent variable and each explanatory variable. [b] Probability and Robust Probability (Robust_Pr): An asterisk (*) indicates a statistically significant coefficient (*p* < 0.01). [c] Variance Inflation Factor (VIF): Values greater than 7.5 imply duplication in explanatory variables.

References

1. Alcoforado, M.J.; Andrade, H. Global Warming and the Urban Heat Island. In *Urban Ecology: An International Perspective on the Interaction Between Humans and Nature*; Springer: Boston, MA, USA, 2008; pp. 249–262. [CrossRef]
2. Yadav, N.; Wu, J.; Banerjee, A.; Pathak, S.; Garg, R.D.; Yao, S. Climate Uncertainty and Vulnerability of Urban Flooding Associated with Regional Risk Using Multi-Criteria Analysis in Mumbai, India. *Environ. Res.* **2024**, *244*, 117962. [CrossRef]
3. Gao, S.; Zhan, Q.; Yang, C.; Liu, H. The Diversified Impacts of Urban Morphology on Land Surface Temperature among Urban Functional Zones. *Int. J. Environ. Res. Public Health* **2020**, *17*, 9578. [CrossRef]
4. McNabb, D.E.; McNabb, D.E. The Population Growth Barrier. In *Global Pathways to Water Sustainability*; Palgrave Macmillan: Cham, Switzerland, 2019; pp. 67–81. [CrossRef]
5. Li, X.; Stringer, L.C.; Dallimer, M. The Impacts of Urbanisation and Climate Change on the Urban Thermal Environment in Africa. *Climate* **2022**, *10*, 164. [CrossRef]
6. Simpson, C.H.; Brousse, O.; Heaviside, C. Estimated Mortality Attributable to the Urban Heat Island during the Record-Breaking 2022 Heatwave in London. *Environ. Res. Lett.* **2024**, *19*, 94047. [CrossRef]
7. Lauwaet, D.; Berckmans, J.; Hooyberghs, H.; Wouters, H.; Driesen, G.; Lefebre, F.; De Ridder, K. High Resolution Modelling of the Urban Heat Island of 100 European Cities. *Urban Clim.* **2024**, *54*, 101850. [CrossRef]
8. Zwolska, A.; Półrolniczak, M.; Kolendowicz, L. Urban Growth's Implications on Land Surface Temperature in a Medium-Sized European City Based on LCZ Classification. *Sci. Rep.* **2024**, *14*, 8308. [CrossRef]
9. Ulpiani, G. On the Linkage between Urban Heat Island and Urban Pollution Island: Three-Decade Literature Review towards a Conceptual Framework. *Sci. Total Environ.* **2021**, *751*, 141727. [CrossRef]
10. Cavan, G.; Lindley, S.; Jalayer, F.; Yeshitela, K.; Pauleit, S.; Renner, F.; Gill, S.; Capuano, P.; Nebebe, A.; Woldegerima, T. Urban Morphological Determinants of Temperature Regulating Ecosystem Services in Two African Cities. *Ecol. Indic.* **2014**, *42*, 43–57. [CrossRef]
11. Sahu, P.; Debsarma, C. Climate Change and Urban Environment Sustainability: Issues and Challenges. *Clim. Chang. Urban Environ. Sustain.* **2023**, 1–13. [CrossRef]
12. Koop, S.H.A.; van Leeuwen, C.J. The Challenges of Water, Waste and Climate Change in Cities. *Environ. Dev. Sustain.* **2017**, *19*, 385–418. [CrossRef]
13. Amir Siddique, M.; Boqing, F.; Dongyun, L. Modeling the Impact and Risk Assessment of Urbanization on Urban Heat Island and Thermal Comfort Level of Beijing City, China (2005–2020). *Sustainability* **2023**, *15*, 6043. [CrossRef]
14. Abd-Elmabod, S.K.; Jiménez-González, M.A.; Jordán, A.; Zhang, Z.; Mohamed, E.S.; Hammam, A.A.; El Baroudy, A.A.; Abdel-Fattah, M.K.; Abdelfattah, M.A.; Jones, L. Past and Future Impacts of Urbanisation on Land Surface Temperature in Greater Cairo over a 45 Year Period. *Egypt. J. Remote Sens. Space Sci.* **2022**, *25*, 961–974.
15. Fu, P.; Weng, Q. A Time Series Analysis of Urbanization Induced Land Use and Land Cover Change and Its Impact on Land Surface Temperature with Landsat Imagery. *Remote Sens. Environ.* **2016**, *175*, 205–214. [CrossRef]
16. Gohain, K.J.; Mohammad, P.; Goswami, A. Assessing the Impact of Land Use Land Cover Changes on Land Surface Temperature over Pune City, India. *Quat. Int.* **2021**, *575*, 259–269. [CrossRef]
17. Imran, M.; Mehmood, A. Analysis and Mapping of Present and Future Drivers of Local Urban Climate Using Remote Sensing: A Case of Lahore, Pakistan. *Arab. J. Geosci.* **2020**, *13*, 278. [CrossRef]
18. Kafy, A.-A.; Shuvo, R.M.; Naim, M.N.H.; Sikdar, M.S.; Chowdhury, R.R.; Islam, M.A.; Sarker, M.H.S.; Khan, M.H.H.; Kona, M.A. Remote Sensing Approach to Simulate the Land Use/Land Cover and Seasonal Land Surface Temperature Change Using Machine Learning Algorithms in a Fastest-Growing Megacity of Bangladesh. *Remote Sens. Appl. Soc. Environ.* **2021**, *21*, 100463. [CrossRef]
19. Abou Samra, R.M. Dynamics of Human-Induced Lakes and Their Impact on Land Surface Temperature in Toshka Depression, Western Desert, Egypt. *Environ. Sci. Pollut. Res.* **2022**, *29*, 20892–20905. [CrossRef] [PubMed]
20. Halder, B.; Bandyopadhyay, J.; Banik, P. Monitoring the Effect of Urban Development on Urban Heat Island Based on Remote Sensing and Geo-Spatial Approach in Kolkata and Adjacent Areas, India. *Sustain. Cities Soc.* **2021**, *74*, 103186. [CrossRef]
21. Gupta, R.; Sharma, M.; Singh, G.; Joshi, R.K. Characterizing Urban Growth and Land Surface Temperature in the Western Himalayan Cities of India Using Remote Sensing and Spatial Metrics. *Front. Environ. Sci.* **2023**, *11*, 1122935. [CrossRef]
22. Sresto, M.A.; Siddika, S.; Fattah, M.A.; Morshed, S.R.; Morshed, M.M. A GIS and Remote Sensing Approach for Measuring Summer-Winter Variation of Land Use and Land Cover Indices and Surface Temperature in Dhaka District, Bangladesh. *Heliyon* **2022**, *8*, e10309. [CrossRef] [PubMed]
23. Guo, L.; Di, L.; Zhang, C.; Lin, L.; Chen, F.; Molla, A. Evaluating Contributions of Urbanization and Global Climate Change to Urban Land Surface Temperature Change: A Case Study in Lagos, Nigeria. *Sci. Rep.* **2022**, *12*, 14168. [CrossRef]
24. Kalyan, S.; Pathak, B. Urban Sprawl Impact Assessment on the Land Surface Temperature over the Green Capital of Gujarat Using a Geospatial Approach. *Environ. Monit. Assess.* **2024**, *196*, 1–20. [CrossRef] [PubMed]
25. Mustafa, E.K.; Liu, G.; Abd El-Hamid, H.T.; Kaloop, M.R. Simulation of Land Use Dynamics and Impact on Land Surface Temperature Using Satellite Data. *GeoJournal* **2021**, *86*, 1089–1107. [CrossRef]

26. Zhao, C.; Zhu, H.; Zhang, S.; Jin, Z.; Zhang, Y.; Wang, Y.; Shi, Y.; Jiang, J.; Chen, X.; Liu, M. Long-term Trends in Surface Thermal Environment and Its Potential Drivers along the Urban Development Gradients in Rapidly Urbanizing Regions of China. *Sustain. Cities Soc.* **2024**, *105*, 105324. [CrossRef]

27. Zhang, H.; Qi, Z.; Ye, X.; Cai, Y.; Ma, W.; Chen, M. Analysis of Land Use/Land Cover Change, Population Shift, and Their Effects on Spatiotemporal Patterns of Urban Heat Islands in Metropolitan Shanghai, China. *Appl. Geogr.* **2013**, *44*, 121–133. [CrossRef]

28. Seun, A.I.; Ayodele, A.P.; Koji, D.; Akande, S.O. The Potential Impact of Increased Urbanization on Land Surface Temperature over South-West Nigeria. *Curr. Res. Environ. Sustain.* **2022**, *4*, 100142. [CrossRef]

29. Moazzam, M.F.U.; Doh, Y.H.; Lee, B.G. Impact of Urbanization on Land Surface Temperature and Surface Urban Heat Island Using Optical Remote Sensing Data: A Case Study of Jeju Island, Republic of Korea. *Build. Environ.* **2022**, *222*, 109368. [CrossRef]

30. Srikanth, K.; Swain, D. Urbanization and Land Surface Temperature Changes over Hyderabad, a Semi-Arid Mega City in India. *Remote Sens. Appl. Soc. Environ.* **2022**, *28*, 100858. [CrossRef]

31. Du, C.; Song, P.; Wang, K.; Li, A.; Hu, Y.; Zhang, K.; Jia, X.; Feng, Y.; Wu, M.; Qu, K. Investigating the Trends and Drivers between Urbanization and the Land Surface Temperature: A Case Study of Zhengzhou, China. *Sustainability* **2022**, *14*, 13845. [CrossRef]

32. Chao, L.; Li, Q.; Dong, W.; Yang, Y.; Guo, Z.; Huang, B.; Zhou, L.; Jiang, Z.; Zhai, P.; Jones, P. Vegetation Greening Offsets Urbanization-Induced Fast Warming in Guangdong, Hong Kong, and Macao Region (GHMR). *Geophys. Res. Lett.* **2021**, *48*, e2021GL095217. [CrossRef]

33. Wang, N.; Chen, J.; He, T.; Xu, X.; Liu, L.; Sun, Z.; Qiao, Z.; Han, D. Understanding the Differences in the Effect of Urbanization on Land Surface Temperature and Air Temperature in China: Insights from Heatwave and Non-Heatwave Conditions. *Environ. Res. Lett.* **2023**, *18*, 104038. [CrossRef]

34. Yu, S.; Zhu, Z.; Zhang, Z.; Cai, S.; Liu, F.; Zhao, X.; Wang, X.; Hu, S. Land Surface Temperature Changes in Different Urbanization Increments in China since 2000. *Land* **2024**, *13*, 417. [CrossRef]

35. Shu, B.; Chen, Y.; Zhang, K.; Dehghanifarsani, L.; Amani-Beni, M. Urban Engineering Insights: Spatiotemporal Analysis of Land Surface Temperature and Land Use in Urban Landscape. *Alexandria Eng. J.* **2024**, *92*, 273–282. [CrossRef]

36. Wang, Y.; Xie, X.; Zhao, X.; Liang, S.; Zhu, B.; Tursun, A.; Jiang, F.; Liu, Y.; Zhang, X. Four-Decade Response of Land Surface Temperature to Urban Expansion in Beijing. *Agric. For. Meteorol.* **2023**, *341*, 109653. [CrossRef]

37. Xiang, X.; Zhai, Z.; Fan, C.; Ding, Y.; Ye, L.; Li, J. Modelling Future Land Use Land Cover Changes and Their Impacts on Urban Heat Island Intensity in Guangzhou, China. *J. Environ. Manag.* **2024**, *366*, 121787. [CrossRef] [PubMed]

38. Sun, Y.; Zhang, X.; Ren, G.; Zwiers, F.W.; Hu, T. Contribution of Urbanization to Warming in China. *Nat. Clim. Chang.* **2016**, *6*, 706–709. [CrossRef]

39. Hu, M. Urbanization in Beijing: Challenges and Sustainable Solutions for Water Scarcity and Urban Heat Islands. *Highlights Sci. Eng. Technol.* **2024**, *86*, 108–114. [CrossRef]

40. Cao, J.; Zhou, W.; Yu, W.; Hu, X.; Yu, M.; Wang, J.; Wang, J. Urban Expansion Weakens the Contribution of Local Land Cover to Urban Warming. *Urban Clim.* **2022**, *45*, 101285. [CrossRef]

41. Guo, X.; Fu, D.; Wang, J. Mesoscale Convective Precipitation System Modified by Urbanization in Beijing City. *Atmos. Res.* **2006**, *82*, 112–126. [CrossRef]

42. Zhang, Z.; Li, N.; Wang, X.; Liu, F.; Yang, L. A Comparative Study of Urban Expansion in Beijing, Tianjin and Tangshan from the 1970s to 2013. *Remote Sens.* **2016**, *8*, 496. [CrossRef]

43. Chen, J.; Gong, P.; He, C.; Pu, R.; Shi, P. Land-Use/Land-Cover Change Detection Using Improved Change-Vector Analysis. *Photogramm. Eng. Remote Sens.* **2003**, *69*, 369–379. [CrossRef]

44. Wu, Q.; Li, H.; Wang, R.; Paulussen, J.; He, Y.; Wang, M.; Wang, B.; Wang, Z. Monitoring and Predicting Land Use Change in Beijing Using Remote Sensing and GIS. *Landsc. Urban Plan.* **2006**, *78*, 322–333. [CrossRef]

45. He, C.; Okada, N.; Zhang, Q.; Shi, P.; Li, J. Modelling Dynamic Urban Expansion Processes Incorporating a Potential Model with Cellular Automata. *Landsc. Urban Plan.* **2008**, *86*, 79–91. [CrossRef]

46. He, C.; Wei, A.; Shi, P.; Zhang, Q.; Zhao, Y. Detecting Land-Use/Land-Cover Change in Rural–Urban Fringe Areas Using Extended Change-Vector Analysis. *Int. J. Appl. Earth Obs. Geoinf.* **2011**, *13*, 572–585. [CrossRef]

47. Du, J.; Thill, J.-C.; Peiser, R.B.; Feng, C. Urban Land Market and Land-Use Changes in Post-Reform China: A Case Study of Beijing. *Landsc. Urban Plan.* **2014**, *124*, 118–128. [CrossRef]

48. Beijing Statistical Yearbook. Available online: https://nj.tjj.beijing.gov.cn/nj/main/2023-tjnj/zk/indexeh.htm (accessed on 25 September 2024).

49. Wang, Y.; Xie, X.; Liang, S.; Zhu, B.; Yao, Y.; Meng, S.; Lu, C. Quantifying the Response of Potential Flooding Risk to Urban Growth in Beijing. *Sci. Total Environ.* **2020**, *705*, 135868. [CrossRef]

50. Ji, Y.; Jin, J.; Zhan, W.; Guo, F.; Yan, T. Quantification of Urban Heat Island-Induced Contribution to Advance in Spring Phenology: A Case Study in Hangzhou, China. *Remote Sens.* **2021**, *13*, 3684. [CrossRef]

51. Tian, H.; Liu, L.; Zhang, Z.; Chen, H.; Zhang, X.; Wang, T.; Kang, Z. Spatiotemporal Differentiation and Attribution of Land Surface Temperature in China in 2001–2020. *J. Geogr. Sci.* **2024**, *34*, 375–396. [CrossRef]

52. Agrawal, Y.; Pandey, H.; Tiwari, P.S. An Analytical Study of Relation between Land Surface Temperature and Land Use/Land Cover Using Spectral Indices: A Case Study of Chandigarh. *J. Geomat.* **2023**, *17*, 184–197. [CrossRef]

53. Nganyiyimana, J.; Ngarambe, J.; Yun, G.Y. Nighttime Light: A Potential Proxy for Local Nocturnal Urban Heat Island Intensity in Seoul. *J. Green Build.* **2023**, *18*, 29–41. [CrossRef]

54. Guha, S.; Govil, H.; Mukherjee, S. Impact of Seasonality and Land Use Changes on Urban Heat Island Using Earth-Observing Satellites. In *Earth Observation in Urban Monitoring*; Elsevier: Amsterdam, The Netherlands, 2024; pp. 133–153.

55. Torres-Rojas, L.; Chaney, N.W. A Comprehensive Global Analysis of the Spatiotemporal Variability of Land Surface Temperature. In Proceedings of the EGU23, the 25th EGU General Assembly, Vienna, Austria, 23–28 April 2023; p. EGU-10031.

56. Firozjaei, M.K.; Mijani, N.; Kiavarz, M.; Duan, S.-B.; Atkinson, P.M.; Alavipanah, S.K. A Novel Surface Energy Balance-Based Approach to Land Surface Temperature Downscaling. *Remote Sens. Environ.* **2024**, *305*, 114087. [CrossRef]

57. Shen, Z.; Zeng, J. Spatial Relationship of Urban Development to Land Surface Temperature in Three Cities of Southern Fujian. *Acta Geogr. Sin.* **2021**, *76*, 566–583.

58. Lian, D.; Yuan, B.; Li, X.; Shi, Z.; Ma, Q.; Hu, T.; Miao, S.; Huang, J.; Dong, G.; Liu, Y. The Contrasting Trend of Global Urbanization-Induced Impacts on Day and Night Land Surface Temperature from a Time-Series Perspective. *Sustain. Cities Soc.* **2024**, *109*, 105521. [CrossRef]

59. Ban, Y.; Liu, X.; Yin, Z.; Li, X.; Yin, L.; Zheng, W. Effect of Urbanization on Aerosol Optical Depth over Beijing: Land Use and Surface Temperature Analysis. *Urban Clim.* **2023**, *51*, 101655. [CrossRef]

60. Zhang, H.; Yin, Y.; An, H.; Lei, J.; Li, M.; Song, J.; Han, W. Surface Urban Heat Island and Its Relationship with Land Cover Change in Five Urban Agglomerations in China Based on GEE. *Environ. Sci. Pollut. Res.* **2022**, *29*, 82271–82285. [CrossRef] [PubMed]

61. Sarker, T.; Fan, P.; Messina, J.P.; Macatangay, R.; Varnakovida, P.; Chen, J. Land Surface Temperature and Transboundary Air Pollution: A Case of Bangkok Metropolitan Region. *Sci. Rep.* **2024**, *14*, 10955. [CrossRef]

62. Chen, H.; Liu, L.; Zhang, Z.; Liu, Y.; Tian, H.; Kang, Z.; Wang, T.; Zhang, X. Spatio-Temporal Correlation between Human Activity Intensity and Land Surface Temperature on the North Slope of Tianshan Mountains. *J. Geogr. Sci.* **2022**, *32*, 1935–1955. [CrossRef]

63. Abdulmana, S.; Prasetya, T.A.E.; Garcia-Constantino, M.; Lim, A. Statistical Modeling for Forecasting Land Surface Temperature Increase in Taiwan from 2000 to 2023 Using Three Knots Cubic Spline. *Model. Earth Syst. Environ.* **2024**, *10*, 2793–2801. [CrossRef]

64. Jiang, J.; Johansen, K.; Tu, Y.-H.; McCabe, M.F. Multi-Sensor and Multi-Platform Consistency and Interoperability between UAV, Planet CubeSat, Sentinel-2, and Landsat Reflectance Data. *GIScience Remote Sens.* **2022**, *59*, 936–958. [CrossRef]

65. Obata, K.; Yoshioka, H. Unmixing-Based Radiometric and Spectral Harmonization for Consistency of Multi-Sensor Reflectance Time-Series Data. *ISPRS J. Photogramm. Remote Sens.* **2024**, *212*, 396–411. [CrossRef]

66. Hurtt, G.C.; Chini, L.; Sahajpal, R.; Frolking, S.; Bodirsky, B.L.; Calvin, K.; Doelman, J.C.; Fisk, J.; Fujimori, S.; Goldewijk, K.K. Harmonization of Global Land-Use Change and Management for the Period 850–2100 (LUH2) for CMIP6. *Geosci. Model Dev. Discuss.* **2020**, *13*, 5425–5464. [CrossRef]

67. Liu, F.; Hou, H.; Murayama, Y. Spatial Interconnections of Land Surface Temperatures with Land Cover/Use: A Case Study of Tokyo. *Remote Sens.* **2021**, *13*, 610. [CrossRef]

68. Lamarche, C.; Bontemps, S.; Verhegghen, A.; Radoux, J.; Vanbogaert, E.; Kalogirou, V.; Seifert, F.M.; Arino, O.; Defourny, P. Characterizing the Surface Dynamics for Land Cover Mapping: Current Achievements of the ESA CCI Land Cover. In Proceedings of the Proc. ESA Living Planet Symposium, Edinburgh, UK, 9–13 September 2013; pp. 9–13.

69. Land Cover CCI: Product User Guide Version 2.0. 2017. Available online: https://scholar.archive.org/work/4ozs3 fmdxzbfvdbqmnk2dvxesy/access/wayback/http://maps.elie.ucl.ac.be/CCI/viewer/download/ESACCI-LC-Ph2-PUGv2_2 .0.pdf (accessed on 15 February 2024).

70. Li, W.; Ciais, P.; MacBean, N.; Peng, S.; Defourny, P.; Bontemps, S. Major Forest Changes and Land Cover Transitions Based on Plant Functional Types Derived from the ESA CCI Land Cover Product. *Int. J. Appl. Earth Obs. Geoinf.* **2016**, *47*, 30–39. [CrossRef]

71. Jiang, L.; Yu, L. Analyzing Land Use Intensity Changes within and Outside Protected Areas Using ESA CCI-LC Datasets. *Glob. Ecol. Conserv.* **2019**, *20*, e00789. [CrossRef]

72. Wu, Y.; Tang, Z.; Xiong, S. A Unified Geographically Weighted Regression Model. *Spat. Stat.* **2023**, *55*, 100753. [CrossRef]

73. He, J.; Wei, Y.; Yu, B. Geographically Weighted Regression Based on a Network Weight Matrix: A Case Study Using Urbanization Driving Force Data in China. *Int. J. Geogr. Inf. Sci.* **2023**, *37*, 1209–1235. [CrossRef]

74. Kiani, B.; Sartorius, B.; Lau, C.L.; Bergquist, R. Mastering Geographically Weighted Regression: Key Considerations for Building a Robust Model. *Geospat. Health* **2024**, *19*. [CrossRef]

75. Lessani, M.N.; Li, Z. SGWR: Similarity and Geographically Weighted Regression. *Int. J. Geogr. Inf. Sci.* **2024**, *28*, 1232–1255. [CrossRef]

76. Luo, Y. Spatio-Temporal Analysis of Urban Heat Island in Shanghai over the Past 30 Years with Landsat Images. In Proceedings of the International Conference on Remote Sensing, Surveying, and Mapping (RSSM 2023), Changsha, China, 6–8 January 2023; SPIE: Bellingham, WA, USA, 2023; Volume 12710, pp. 221–227. [CrossRef]

77. Yang, Y.; Guangrong, S.; Chen, Z.; Hao, S.; Zhouyiling, Z.; Shan, Y. Quantitative Analysis and Prediction of Urban Heat Island Intensity on Urban-Rural Gradient: A Case Study of Shanghai. *Sci. Total Environ.* **2022**, *829*, 154264. [CrossRef]

78. Gupta, N.; Aithal, B.H. Effects of Rising Urban Temperatures on the Wellbeing of the Residents: A Case Study of Kolkata Metropolitan Region. *Int. Rev. Spat. Plan. Sustain. Dev.* **2022**, *10*, 79–98. [CrossRef] [PubMed]

79. Wang, Y.-R.; Hessen, D.O.; Samset, B.H.; Stordal, F. Evaluating Global and Regional Land Warming Trends in the Past Decades with Both MODIS and ERA5-Land Land Surface Temperature Data. *Remote Sens. Environ.* **2022**, *280*, 113181. [CrossRef]
80. Yao, N.; van den Bosch, C.C.K.; Yang, J.; Devisscher, T.; Wirtz, Z.; Jia, L.; Duan, J.; Ma, L. Beijing's 50 Million New Urban Trees: Strategic Governance for Large-Scale Urban Afforestation. *Urban For. Urban Green.* **2019**, *44*, 126392. [CrossRef]
81. Hussain, S.; Mubeen, M.; Ahmad, A.; Masood, N.; Hammad, H.M.; Amjad, M.; Imran, M.; Usman, M.; Farid, H.U.; Fahad, S. Satellite-Based Evaluation of Temporal Change in Cultivated Land in Southern Punjab (Multan Region) through Dynamics of Vegetation and Land Surface Temperature. *Open Geosci.* **2021**, *13*, 1561–1577. [CrossRef]